Full-Wave Planar Near-Field Measurement Simulation Using Vivaldi Antenna as a Probe

R. F. Dubrovka[1],
R.C. Jones[1], C.G. Parini[1].
[1]School of Electronic Engineering and Computer Sciences
Queen Mary University of London
London, E1 4NS, UK
r.dubrovka@qmul.ac.uk

S.F. Gregson[1,2], *Fellow, AMTA*.
[2]Next Phase Measurements
CA, USA
stuart.gregson@npmeas.com

***Abstract*— In this paper, a new approach for planar near-field (NF) measurements for lower band 5G applications is presented employing a customised Vivaldi antenna as a near-field probe. The paper includes a careful analysis of the impact that the absorber collar has on the overall measurement performance of the probe. A 5G, 24-elements, C-band, planar array antenna has been used as an antenna under test (AUT). Full-wave three-dimensional computational electromagnetic simulations (CEM) of the production test, measurement, and calibration of a given planar-near-field measurement setup with, and without, absorber collar, have been undertaken. Here, special attention has been paid to a thorough examination of the presence of scattering, and the standing waves in the simulated near-field measurement. The presence and impact of this phenomenon has been carefully inspected by intensive simulations and compared with results obtained for a standard open-ended waveguide probe (OEWG) probe, as well as with an alternative dielectric probe. The obtained results have demonstrated clear advantages when compared to the alternative solutions with superior results being obtained in terms of the scattering performance. Standing waves and ripple are found to be far less visible with the overall results after probe compensation being noticeably improved when compared with the more commonly used alternatives. We complete this study by verifying the suitability of the proposed Vivaldi probe for Spherical NF measurements by comparing its spherical mode coefficients with that of the ubiquitous OEWG. In conclusion, the Vivaldi probe spans several waveguide bands, and is suitable for planar, cylindrical, and spherical near-field testing applications.**

Index Terms*— *Planar Near-Field, Probe, Broadband, Low Scattering, Measurement Simulation.

I. INTRODUCTION

Near-field measurements have become an indispensable part of modern antenna design and measurement [1, 2]. Very often, rectangular open-ended rectangular waveguide (OEWG) probes are used to acquire near-field data [1, 2]. Unfortunately however, these devices are band-limited, have not inconsiderable scattering cross-sections [2, 3], and at low frequencies they tend to become excessively large, bulky, and heavy, and at higher frequencies they can become impractically small, delicate, and become difficult to align. This is equally true of pyramidal horns, *e.g.,* standard gain horns (SGH) [1, 4], which can also be used as probes in free-field testing applications when more gain is required to improve the overall RF power budget.

To overcome the aforementioned, well recognised, disadvantages; a customised Vivaldi antenna has been introduced as a near-field probe. The advantage that this sort of open-boundary antenna offers is twofold. Firstly, the operational frequency band exceeds that of a single, standard, rectangular waveguide [1], and secondly the Vivaldi antenna (has no need for a ground-plane, or a cavity backing) possesses a very small amount of physical structure with which to scatter an incoming illuminating field. This offers the potential for delivering a very practical measurement probe, that is also potentially, minimally invasive. It is also recognised that the design of the absorber collar can have a significant impact on the electrical performance of low-gain, near-field probe antennas [5]. Thus, this study included the examination of several possible measurement scenarios, and a careful analysis of the impact that the absorber collar has on the overall measurement performance of the probe [5]. This took a similar approach to the authors prior work [6], and centred upon the measurement of an FR1, 5G, C-band, 24-element, planar Massive MIMO antenna which was employed as the antenna under test (AUT). Here, full-wave, three-dimensional, computational electromagnetic simulations (CEM) of the production test, measurements, and calibration of the given planar-near-field measurement setup with, and without, absorber collar, have been undertaken.

In order to perform such complex and high resource intensive evaluation, a proprietary full-wave CEM solver (Altair FEKO [7], in the following text – simply FEKO) has been used running on a large, parallel, computing cluster. Here, special attention, analogous to the authors' previous work [6], has been paid to a thorough examination of the presence of scattering, and the standing waves within the simulated near-field measurement. Intensive simulations in comparison with results obtained for a standard OEWG probe, as well as with an alternative dielectric probe [8], have been undertaken to carefully investigate the presence and impact of this aforementioned phenomenon. Noticeable overall improvement of all characteristics and performance of the introduced probe are demonstrated with the proposed probe being suitable for planar, cylindrical, and spherical near-field testing applications [1].

The structure of the paper is as follows, Section II provides an overview of the CEM modelling. Section III gives a reader an insight into the simulated NF "experiment" and obtained results. In Section IV the possibility of using the presented antenna as a probe for spherical near-field (SNF) scanning is discussed. Lastly, the paper finishes with the summary and conclusions.

II. Full 3-D Modelling of the Experiment

In order to numerically recreate the experiment, a complete three-dimensional model of the AUT and probe was generated. As in [6], the AUT comprised a 24-element planar array antenna operating in C-band. This can be seen presented in Figure 1 together with its predicted far-field radiation pattern (RP). In the same way as in the previous work, the array was fed by an ideal network with equal phase and amplitude excitations. The array consisted of 24 identical, pin-fed, patch antennas. As the near-field and far-field performance has been demonstrated in [6], it is not repeated here due to the limitation of available space.

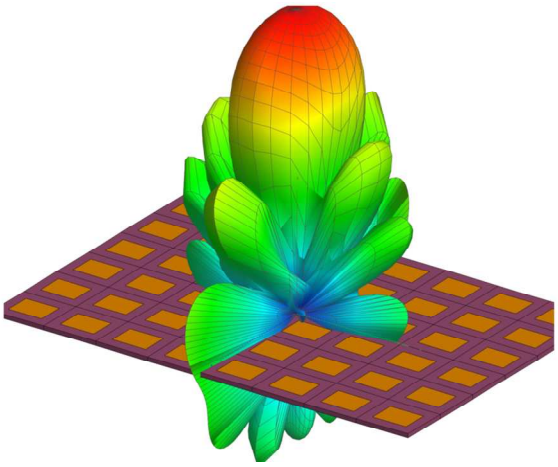

Figure 1. Mechanical drawing of AUT, C-band Massive MIMO array shown together with far-field radiation pattern.

As explained above, in this study the near-field probe comprised a small Vivaldi antenna which was adapted from standard designs, *cf.* [9]. The Vivaldi antenna was adapted for the desired frequency range and is illustrated in Figure 2 where it is shown without (a) and with (b) the absorber collar.

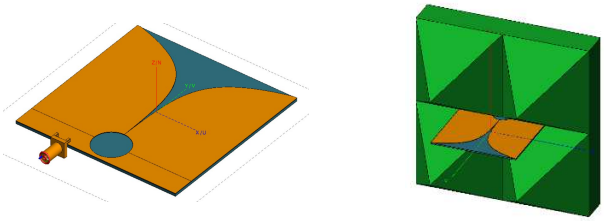

(a) (b)

Figure 2. Overall view of the Vivaldi Antenna.

Here, the CEM model of the Vivaldi antenna includes both the matching and radiating portions which increases the complexity of the model but ensures greater accuracy when examining the scattering properties of the antenna. For the presented work, the antenna was realised using an FR-4 substrate with a dielectric constant of 4.4. The Vivaldi antenna was inserted into a rectangular block of pyramidal absorber, Figure 2b, where the absorber properties were modelled on values found in the open literature, *e.g.,* [10]. In order to match the antenna design to the frequency band of interest, which was in this case centred at 3.5 GHz, the feed arrangement was modified, which finally yielded a VSWR value of better than 1.2 between 3.21 and 3.64 GHz. Figure 3 demonstrates two cardinal cuts $\varphi = 0°$ and $\varphi = 90°$ of the far-field radiation pattern of the antenna with the absorber collar. Here, the blue traces represent the pattern of the Vivaldi probe when embedded in absorber, and the green trace denotes the case when the Vivaldi was in free-space. From Figure 3, it is seen that absorber has a notable influence on the behaviour of the antenna. From inspection we see that the absorber significantly improves the symmetry of the radiation pattern. The reason for this is that although the Vivaldi is symmetrical at the aperture, a stand-alone Vivaldi antenna has a matching and feeding structure which is asymmetrical, and which will affect the radiated field distribution. However, it must be noted that in doing this, there was small loss of gain. Nevertheless, gain in and of itself was not a parameter that was of primary concern in this study. At these frequencies, the RF power budget can routinely be expected to be *circa* 80 dB, which will be more than sufficient to render this small loss of sensitivity unimportant.

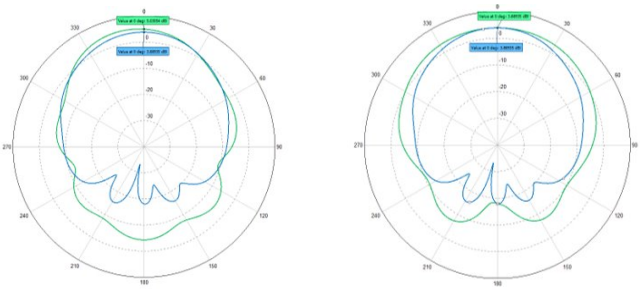

(a) Cut at $\phi = 0°$ (b) Cut at $\phi = 90°$

Figure 3. Cardinal cuts of the far-field radiation pattern of the Vivaldi antenna with and without absorber.

Finally, the optimised near-field probe was placed above the AUT, and near-field data was "acquired" in a numerical experiment which comprised a digital twin of a typical planar-near-field acquisition providing far-field data over a span of *circa* 120° [1, 4]. The sampling step in both directions was 40mm which is slightly less than half-wavelength at the operating frequency of 3.5 GHz. The near-field measurement plane was placed at a distance of 460 mm, which is approximately five wavelengths, a fairly typical AUT-to-probe separation that could be used in a practical measurement, and which is large enough to ensure that reactive, evanescent, fields are well attenuated, and therefore absent from the simulated measurement. Here, each and every point within the PNF measurement comprised an individual, complete, full-wave, three-dimensional method-of-moments (MoM) CEM simulation of the AUT and probe pair. This requirement was the main driver behind the computational size of this problem and was the reason the simulations were undertaken using a large computing cluster which had 512 GB RAM, 32 CPU cores running at 2.2 GHz, and 64 logical processors. Here, the

Method of Moment (MoM) was selected as it avoids the need to mesh a vacuum and is therefore amenable to taking physically large problems such the simulation of a large PNF acquisition. This simulated planar near-field data was transformed to the far-field using a standard probe-corrected transform with the far-field pattern of the Vivaldi probe being utilised for the probe compensation with the transformed simulated "measured" data shown in Figure 4.

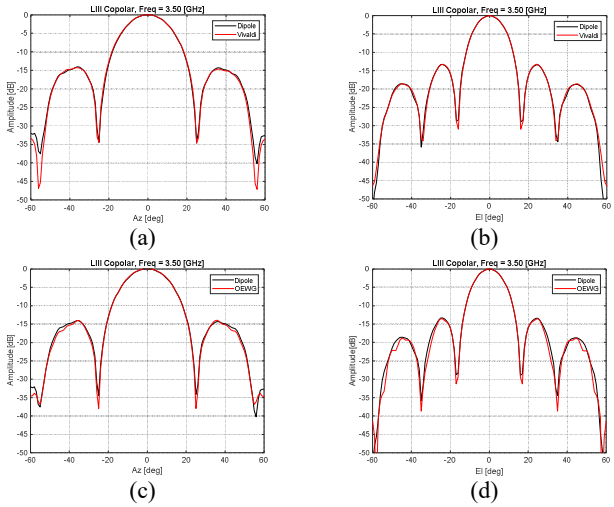

Figure 4. Re-combined far-field radiation patterns of the AUT probed with the Vivaldi antenna and the OEWG probe [9] in comparison with the pure NF measurements: (a) Vivaldi azimuth cut, (b) Vivaldi elevation cut, (c) OEWG azimuth cut, and (d) OEWG elevation cut.

Here, one can see a small difference between the respective transformed far-field radiation patterns created by a conversion of near-field numerical scanning of the probe antenna, a Vivaldi antenna in this case; and the near-field scan of the AUT, measured at the same distance using a Hertzian dipole probe. These differences are a result of differences in the truncation between the two measurements. Gibb's ripple, *i.e.*, spectral leakage [11], will be different between the two data sets as the spatial near-field data will be different. Although probe pattern compensation is applied correcting for pattern and polarisation of the probe, it is applied in the far-field, after the Gibb's effects are introduced by the transform and are already present within the data, and then only their general level will be adjusted by the far-field probe pattern. However, from comparison with Figure 4c) and d), which was obtained previously (Figure 9 of [6]) when using a conventional rectangular open-ended rectangular waveguide (OEWG) probe, the degree of agreement attained here is considerably improved over that.

As noted above, in addition to the broad band of the Vivaldi probe, another desirable attribute is the comparatively low scattering cross-section and the reduction in the amplitude of the standing waves that are present between probe and AUT. These are of more concern in a planar measurement due to the comparatively short-range length and are excluded from standard near-field to far-field transforms with their effect being included instead as a component in the facility level uncertainty budget [1, 4]. Thus, as probe compensation does not consider multiple-reflections, and hence minimising the amount of scattering emanating from the near-field probe is clearly desirable. It is important to note at this point that merely optimising the design of a given near-field probe to minimise the radar cross-section (RCS) on or near boresight is insufficient to guarantee a minimum near-field scattering probe. RCS is by virtue of its definition [2] a far-field property assuming plane-wave illumination. Conversely, in the near-field, we can assume that the probe is illuminated simultaneously by an angular spectrum of plane waves all propagating in different directions with different complex amplitudes. Thus, RCS is a far-field parameter, and we are working in the near-field where a clear, direct, one-to-one mapping does not exist. Hence, in this study, we chose to minimise the scattering which we were able to accurately assess through the use of a full-wave simulation that included the waveguide to coaxial transitions on both antennas. Thus, the output of the simulations that was employed here was the port reflection coefficient and the port-to-port transmission scattering coefficient. This is discussed in greater detail below.

III. Scattering Experiment and Results

As noted above, the simulation effort was devoted to assessing the mutual-coupling in the near-field, as opposed to looking purely at far-field RCS, although that was predicted as part of this study. Two simulated experimental procedures were harnessed:

a) Near-field z-axis scan of the AUT with and without the absorbing collar for the OEWG and Vivaldi probes.

b) Simulated classical PNF measurement at two different z-distances (*i.e.*, at z, and at $z + \lambda/4$) to investigate the AUT-to-probe standing wave.

The results of these simulated experiments are presented in the following sections.

A. *Near-Field Z-Scan with and without absorber collar*

Figure 5 presents results of the z-scan experiment with the OEWG and Vivaldi probes which is intended to investigate the standing waves in the respective experimental setups. Here, the probes were in the same x,y position relative to the AUT. Fig. 5 shows a comparison of S_{21} from AUT-to-probe separation of 2λ to 7λ in z with the probes positioned in the centre of the array antenna. Here, each trace has been plotted with and without the absorber collar.

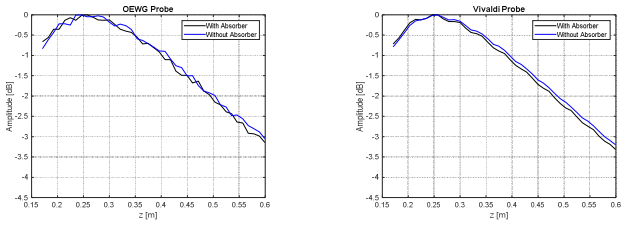

Figure 5. NF z-scan with and without absorber collar for OEWG probe (a), and Vivaldi probe (b).

From Figure 5a we can see that the comparatively small size of the collar has resulted in a relatively small change in scattering performance as measured by the ripple on the respective traces, blue trace denotes without absorber, black

trace is with absorber collar. By comparison of Figure 5a and 5b it can be seen that the best performing probe in terms of multiple reflections is the Vivaldi probe (significantly) bettering the OEWG probe. It is important to note that these are complete full-wave simulations which are taking into account the full properties of both the AUT and probe.

Although this provides a comparative assessment of the mutual coupling between the AUT and probes, a further step is to compare each of the probes, in this case with the absorber collar, against the ideal Hertzian dipole probe. In Figure 6, a normalised transmission coefficient as a function of wavelength is plotted, *i.e.*, plotted relative to an ideal, zero-scattering, Hertzian dipole probe. Typically, PNF measurements would be taken with an AUT-to-probe separation of $3\lambda \leqslant z \leqslant 5\lambda$. Also, an additional plot for a pixelated dielectric probe is demonstrated for the sake of comparison. The dielectric probe [8] measurements are beyond the scope of this paper, however, it is clearly seen that such probe, although praised for its small cross-section, is not the best candidate for NF scanning, as it creates the largest ripples due to multiple reflections existing between the AUT and the probe. The Vivaldi probe has the smallest amplitude ripple, bettering the OEWG probe which is the de facto standard NF probe.

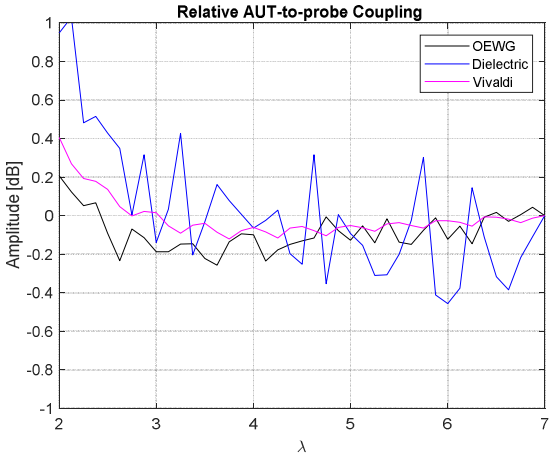

Figure 6. Comparison of AUT-to-probe S_{21} respectively for OEWG, pixilated dielectric, and Vivaldi probe plotted as a function of distance in wavelengths.

In Fig. 6, the magnitude of the ripple (AUT-to-probe multiple reflections) are plotted. Beyond 3λ (typical measurement range length) a ripple of circa: 0.7 dB for the dielectric probe; 0.2 dB for OEWG; and 0.1 dB Vivaldi are observed. Beyond 5λ, the Vivaldi probe has a point-to-point ripple of ~0.03 dB. This is a very low level. In terms of scattering cross-section, the Vivaldi probe has a clear advantage. Thus, the Vivaldi probe is not only broadband (spanning more than a single WG band), is has the best scattering cross-section when used for PNF applications.

B. *Simulation of Two PNF Scans displaced by a quarter of a wavelength in the z-axis*

A standard experimental way to evaluate the multiple-reflection term within a PNF range uncertainty budget [1, 2] is to increase the AUT-to-probe separation by a quarter of a wavelength. This results in a maximum change in the phase of the reflected wave. Transforming these patterns and compensating for the AUT-to-probe separation allows a vector comparison to be made. However, this is computationally very intensive simulation, but it provides the data needed to perform a far-field assessment of the impact that multiple-reflections have on measured antenna parameters. Within this simulation, there will inevitably be some (very) small increase in truncation as the second plane is located further away from the AUT however that change is not expected to be significant in the comparison of this parametric change. The results of this can be seen presented in Figure 7. Here, we see the RMS dB difference level was at -55.17 dB. This corresponds to a level of a little better than ±0.02 dB uncertainty, which is much smaller than we could typically expect to see in a standard PNF range assessment using an OEWG probe [12].

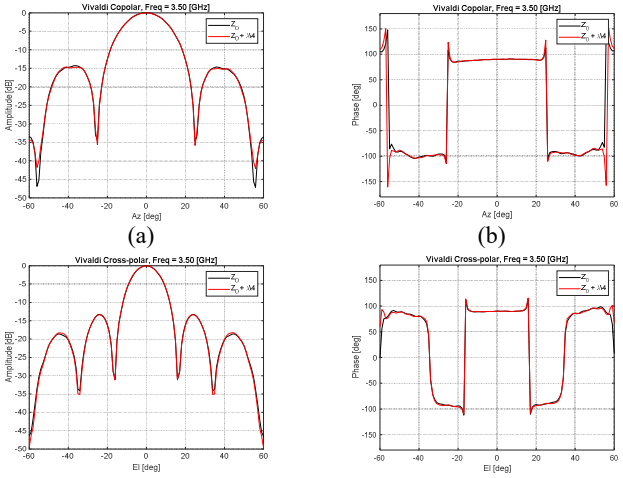

Figure 7. Comparison of far-field patterns taken at z, and $z + \lambda/4$, (a) amplitude azimuth cut, (b) phase azimuth cut, (c) amplitude elevation cut, (d) phase elevation cut.

IV. Examination of Use as a Probe for Spherical Near-Field Scanning

In the preceding sections we have demonstrated the utility of this probe for the purposes of taking minimally invasive, planar near-field measurements. An obvious further question is whether this probe could be used to acquire cylindrical, or spherical, near-field data. Cylindrical near-field theory has a very similar requirement to that of planar near-field. That is, the "two" probes that are used to acquire the two tangential, orthogonal, near-electric-field components must be different from one another. This is often accomplished by rotating the probe about its axis by 90° from when it was used to acquire the horizontal-field and then acquire the vertical-field component. However, this is more for convenience, than as a result of any fundamental theoretical constraint. However, other than the probes being different, and free from nulls in the forward direction, *i.e.,* not to have too much gain, there are no very specific additional requirements. Put another way, the receiving pattern of the probe has a null in some direction, then the far-field pattern of the AUT cannot be reliably determined in that direction, *i.e.,* that the probe must be sensitive to the

plane-wave modes of interest with this being true for both planar and cylindrical implementations.

However, this is not the case for the spherical near-field case where, within the standard theory, a specific additional requirement is imposed that the probe must be a rotationally symmetric, first order probe [1], *and* that the "second" probe must comprise the "first" probe having been rotated by 90° about its axis. Thus, the suitability of the Vivaldi probe will depend upon how well this antenna adheres to the requirement for azimuthal mode purity, and in the case when it doesn't, what level of accuracy is required [1, 13].

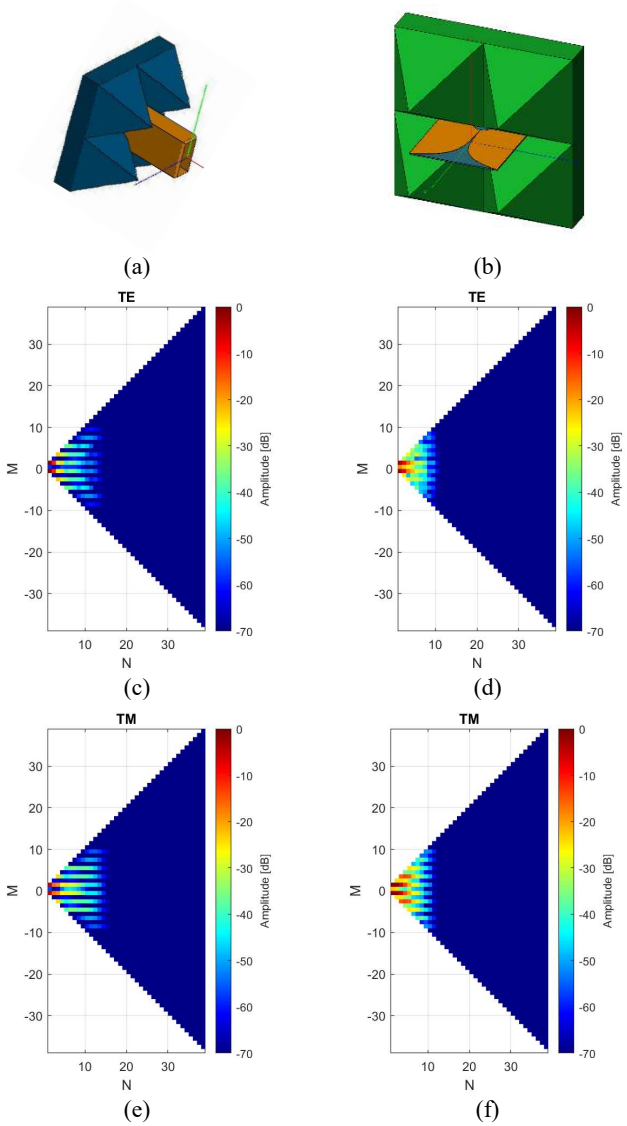

Figure 8. (a) schematic of OEWG probe, (b) schematic of Vivaldi probe, both shown with absorber collars, and a comparison of SMCs for, (c) TE SMCs OEWG, (d) TE SMCs Vivaldi, (e) TM SMCs OEWG, (f) TM SMCs Vivaldi.

It is worth noting that we do have some hope here. If the input probe is a Hertzian dipole probe, *i.e.,* an infinitesimal current element, then probe compensation becomes unnecessary for all forms of near-field antenna measurements. The Vivaldi is an open boundary horn antenna which, from Babinet's principle we know that a thin half-wavelength dipole is the complimentary structure, and so to a first degree this antenna approximates a small dipole quite well. Indeed, this can be evidenced from a comparison of the respective far-field patterns.

As noted above, standard spherical near-field to far-field transforms have the requirement that the probe must be a first order probe [1]. This means that for a probe with azimuthal symmetry, they should have $m = \pm 1$ modes only. This requires near-field measurements at only two χ-angles, *i.e.,* probe rotation angles, 0° and 90°. In Figure 8 we show the computed spherical mode expansion for the Vivaldi probe, and equivalently, for the commonly used rectangular OEWG probe where the coefficients are presented in the form of false color checkerboard plots. From inspection of the spherical mode coefficients (SMC), we can see that the azimuthal modes drop off quickly: *i.e.* the higher order TE modes are more than 24 dB below the first order modes, whilst for the TM modes they are more than 24 dB down (except for the $m = \pm 3$ higher order azimuthal mode. This used the small square absorber collar shown. This performance can probably be improved by redesigning the absorber collar to further improve symmetry in the pattern. By way of a comparison, Figure 8 also contains equivalent SMC plots for a comparable rectangular OEWG probe. Here, we see that the SMC spectrum is broadly comparable with that of the Vivaldi antenna which are routinely used for SNF applications despite not being true "first order" probes. And, over the years, a great deal of time and effort has been devoted to establishing the utility of the OEWG probe for use with spherical applications, *e.g.* [14, 15, 16] and in understanding what those limitations are, and how best to manage them.

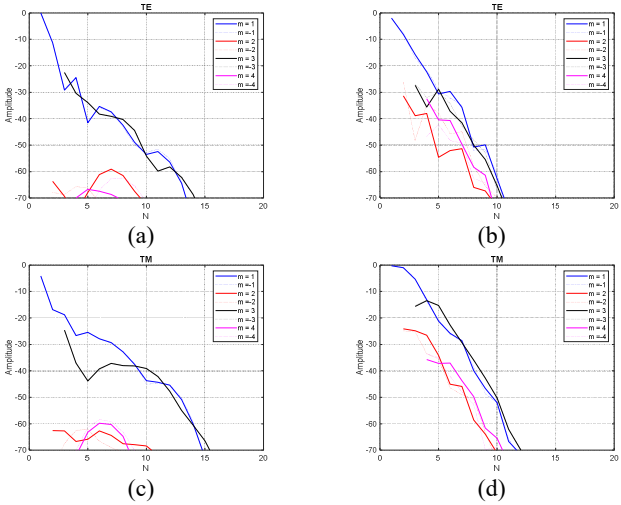

Figure 9. Comparison of SMCs for, (a) TE SMCs OEWG, (b) TE SMCs Vivaldi, (c) TM SMCs OEWG, (d) TM SMCs Vivaldi.

A further illustration of the behaviour of the SMCs, Figure 9 presents plots of the SMCs of both the Vivaldi and rectangular OEWG probe in the form of line graphs. Here it is perhaps easier to see the detail of the lower order azimuthal modes. The OEWG probe clearly has better higher order mode purity than the Vivaldi antenna however, it is also important to note that the TM SMCs of the Vivaldi antenna is in many areas

better than those of the OEWG probe. Thus, although further study is certainly needed, it is very likely that the Vivaldi probe could be successfully used for many SNF testing applications, especially if the measurement radius was on the order of two to four times larger than the maximum radial extent [1], which is also the case when using other broad-band, open boundary type antennas, *e.g.,* dual or quad-ridge horns [1, 15, 16].Specifically, for the case of SNF measurements, if the probe pattern used for spherical processing is changed or the probe correction is neglected, it is the main beam region of the far-field that is affected most, with the sidelobe region being left largely unaffected and, the effect of the higher order mode probe compared to an ideal first order probe decreasing with increasing measurement distance, for a fixed maximum radial extent (MRE), [1, 14, 15, 16]. These studies have also shown that for the case of the OEWG probe, with measurement radii of *circa* twice the MRE, the differences in the near-field and far-field are on the order of -50 dB below the peak amplitudes. However, for larger measurement radii, the differences were found to be typically below -60 dB which is, for a typical spherical near-field measurement, probably below the error levels of other error terms. For the open boundary horn type probes, a measurement radius to MRE ratio of *circa* four was required. It is also important to note that these difference levels are also not highly sensitive to the AUT characteristics, *cf.* [15, 16] where results were presented for the case of a standard gain horn, and a higher gain slotted waveguide array antenna.

CONCLUSIONS

In this paper, a full-wave three-dimensional computational electromagnetic simulations of a C-band 5G Massive MIMO array have been presented. A very good agreement was attained between true and 'measured' far-field results. As was the case with the OEWG probe, the importance of an appropriate absorber collar for the Vivaldi probe has been demonstrated with the level of ripple resulting from reflections between the AUT and probe having been quantified. This paper reports an extension of the authors previous work which provided the baseline performance level for the case of a commonly used OEWG probe. Here, it was shown that the Vivaldi probe outperformed the standard OEWG probe, and an existing low scattering pixilated dielectric probe. It was shown that the Vivaldi probe was able to obtain ~0.02 dB uncertainty in the FF from NF measurements which is much smaller than we typically expect to see in a standard PNF range assessment using OEWG probe. Furthermore, the broadband performance was verified and shown to exceed the bandwidth of a traditional OEWG probe, with performance spanning five standard rectangular WG bands, with a dipole-type pattern function that is suitable for planar, cylindrical and spherical near-field testing applications, as well as for use with far-field multi-probe anechoic chambers (FF-MPAC). The planed future work is to include a further examination of the utility of this probe when taking spherical near-field measurements.

REFERENCES

[1] C. Parini, S. Gregson, J. McCormick, D. Janse van Rensburg and T. Eibert, Theory and Practice of Modern Antenna Range Measurements, 2nd Expanded Edition ed., vol. 1, London: IET Press, 2020.

[2] S.F. Gregson, J. McCormick, C.G. Parini, "Principles of Planar Near-Field Antenna Measurements, 2nd Edition", IET Electromagnetic Waves series 53, ISBN 978-1-83953-699-1, July 2023.

[3] E.H. Ko, D.J. Belgiovane, "Radiation and Scattering Pattern Characteristics of Chamfered-Tip Open-Ended Rectangular Waveguide Probes for Planar Near-Field Antenna Measurement Applications", AMTA, Daytona Beach, FL, October 2021.

[4] C. G. Parini, R. Dubrovka, S. F. Gregson, "Computational Electromagnetic Modelling of Compact Antenna Test Range Quiet Zone Probing", ACES Journal, Vol. 33, No. 2, Feb. 2018.

[5] A Newell, S Gregson, D Gentle, P Miller, "The effect of the absorber collar on open-ended waveguide probes", Antenna Measurement Techniques Association (AMTA), Salt Lake City, Utah, USA, 2009.

[6] R. F. Dubrovka, R. C. Jones, C.G. Parini, S.F. Gregson, "Predication of Planar Near-Field Measurements Based on Full-Wave Three-Dimensional CEM Measurement Simulation," Antenna Measurement Techniques Association (AMTA), Seattle, Washington, USA, 2023.

[7] https://altair.com/feko, accessed 15/07/2024.

[8] H. Lim , H. Park, K.C. Hwang, "A Low-Scattering Pixelated Dielectric Rod Waveguide Probe for Near-Field Measurement", IEEE Trans. Antenna and Prop., Vol. 69, No. 12, Dec. 2021.

[9] B.W. Yicai, J.G. Fang, "Design and Measurement of Compact Tapered Slot Antenna for UWB Microwave Imaging Radar", The Ninth International Conference on Electronic Measurement & Instruments ICEMI 2009.

[10] D. Campbell, G. Gampala, C. J. Reddy, M. Winebrand, and J. Aubin, "Modeling and Analysis of Anechoic Chamber Using CEM Tools", ACES Journal, Vil. 28, No.9, September 2013.

[11] Vretblad, Anders (2000), Fourier Analysis and its Applications, Graduate Texts in Mathematics, vol. 223, New York: Springer Publishing, p. 93, ISBN 978-0-387-00836-3.

[12] A.C. Newell, G.E. Hindman, S.F. Gregson, "Antenna Pattern Comparisons used in NIST I8-Term Error Assessments on Numerous Near-field Ranges", 7th European Conference on Antennas and Propagation, EuCAP 2013.

[13] R.C. Wittmann, M.H. Francis, "Near-Field Spherical Scanning Antenna Measurements: Probe Deconvolution and Sensitivity", Hindawi Publishing Corporation, International Journal of Antennas and Propagation, Volume 2014, Article ID 587874.

[14] A.C. Newell, S.F. Gregson, "Estimating the effect of higher order modes in spherical near-field probe correction", AMTA 34th Annual Meeting & Symposium, Seattle, WA, Oct. 2012.

[15] A.C. Newell, S.F. Gregson, "Higher Order Mode probes in Spherical NearField Measurements", EuCAP, Gothenburg, April, 2013.

[16] A.C. Newell, S.F. Gregson, "Estimating the effect of higher order modes in spherical near-field probe correction", AMTA 35th Annual Meeting & Symposium, Columbus, OH, Oct. 2013.